analytical chemistry

pubs.acs.org/ac

Article

Exploitation of N-Gene of SARS-CoV-2 to Develop a New Rapid Assay by ASOs@AuNPs

Yasaman-Sadat Borghei,* Hamid Reza Samadikhah, and Saman Hosseinkhani*

Cite This: *Anal. Chem.* 2022, 94, 13628−13634

Read Online

ACCESS | Metrics & More | Article Recommendations

ABSTRACT: A naked-eye (equipment-free), label-free (cost-effective), and RNA extraction-free (to speed up) method for SARS-CoV-2 (as a case study of RNA viruses) detection is developed. Here, the DNA is being used as a template for in situ formation of anisotropic gold nanoparticles (AuNPs) without any chemical modification or DNA labeling. In this study, synthesized AuNPs for the direct detection of N-gene (nucleocapsid phosphoprotein) of SARS-CoV-2 are exploited. To this aim, antisense oligonucleotides (ASOs) with an extra poly guanine tail (G12) were designed. Thus, in the presence of its viral target RNA gene and ASOs@AuNPs-RNA hybridization, there was a red shift in its localized surface plasmon resonance (LSPR), and the intensity of the LSPR peak at 690 nm of throat swab samples was compared to the threshold cycle (Ct) of a reverse-transcriptase real-time polymerase chain reaction (RT-qPCR) (as a gold standard). Results suggested that the plasmonic biosensor can detect a very low amount of SARS-CoV-2 with a detection limit close to RT-qPCR. Simplicity of the new conjugation method with hybridization and annealing without amplification and denaturation steps enabled it to perform in a microfluidic paper-based analytical device.

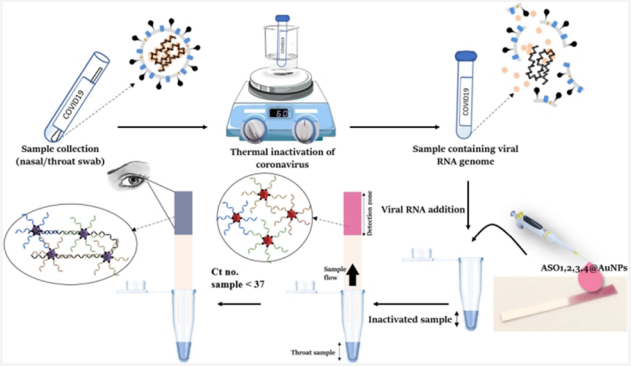

1. INTRODUCTION

Various findings show that human RNA viruses have been involved in causing many epidemics during history like current crisis of SARS-CoV-2 pandemic. Throughout human history, RNA viruses have had great potential for causing infections and pandemics because of their high mutation rate (10^{-3}−10^{-5} errors per nucleotide and replication cycle).[1,2] Some of the most popular of these viruses are Influenza virus, HIV-1, SARS-CoV, Ebola virus, Zika virus, and SARS-CoV-2, the last three of which have emerged in the recent decade, in 2014, 2015, and 2019, respectively.[3,4] The gold standard test for detection of these infectious diseases is the reverse-transcriptase real-time polymerase chain reaction (RT-qPCR). Although this method has maintained its position in clinical diagnostics because of its high sensitivity and specificity, there is wide attention to develop fast, low-cost, RNA extraction-free, and instrument-free methods.[5,6]

Generally, these new approaches of detection are divided into two broad categories. The first category includes PCR-based methods such as the direct-one-step-RT-qPCR assay[5] and loop-mediated isothermal amplification (LAMP) technology.[7] However, the second category includes PCR-free methods and in most cases involves the use of nanomaterials.[8,9]

Among nanomaterials, plasmonic nanoparticles (NPs) have attracted much attention in the field of colorimetric-based assays, in which localized surface plasmon resonance (LSPR) frequency strongly depends on the composition, size, geometry, dielectric environment, and separation distance of NPs.[10,11] How to conjugate different forms of nanomaterials into various biomolecules like proteins and nucleic acids remains a challenge for nanomaterial application. For example, after the first report on conjugation of DNA to gold nanoparticles (AuNPs) by thiolated DNA,[12] it has been optimized in various reports.[13−15] In all of these cases, AuNPs were synthesized with different methods, and then biomolecules like nucleic acids were conjugated to their surface, which is a time-consuming and costly process.

Here, a naked-eye (equipment-free), label-free (cost-effective), and RNA extraction-free (to speed up) method based on LSPR of AuNPs for SARS-CoV-2 (as a case study of RNA viruses) detection has been developed. Thus, we report a single-step and colorimetric assay based on a new in situ synthetic approach for the preparation of polyvalent (p)DNA−

Received: August 13, 2022
Accepted: September 12, 2022
Published: September 21, 2022

Scheme 1. Schematic Representation of μPAD-Based SARS-CoV-2 Colorimetric Assay[a]

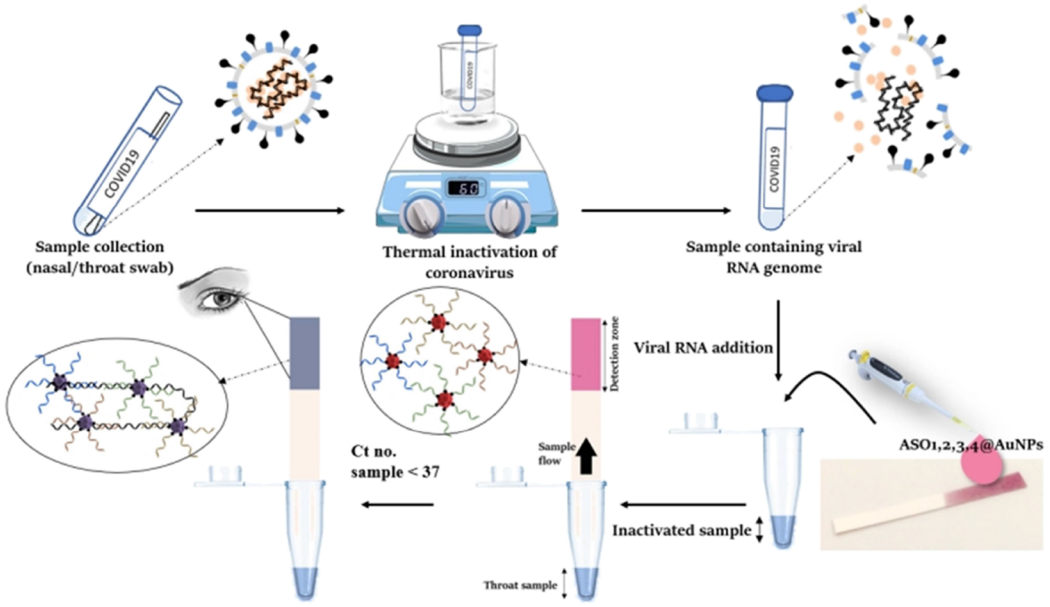

[a]In the first step, the throat swab samples were collected. After thermal inactivation of the viral SARS-CoV-2 samples, in a new microtube, they were mixed with precoated paper with four ASOs@AuNPs, and color changes were observed in less than 5 min.

AuNPs by exploiting an extra strand polyguanine (G_{12}). A specific sequence in the N-gene (nucleocapsid phosphoprotein) of SARS-CoV-2 was selected as a target to design antisense oligonucleotides (ASOs) with an extra strand polyguanine G_{12}. After in situ synthesis of anisotropic AuNPs on four ASOs in a few seconds and formation of polyvalent (p)ASOs@AuNPs, they were added to the inactivated virus sample, and after the annealing process, the color of the solution changed from red to purple. Given that this conjugation method allows hybridization and annealing without a denaturation step, this method was used to perform microfluidic paper-based analytical device (μPAD) assay, and its corresponding color change was visible by the naked eye in the detection zone (Scheme 1).

2. EXPERIMENTAL SECTION

2.1. Materials and Reagents. Chloroauric acid ($HAuCl_4$-$4H_2O$) and HEPES (4-(2-hydroxyethyl)-1-piperazineethanesulfonic acid) were purchased from Sigma-Aldrich. All oligonucleotides used in this work were synthesized by Shanghai Generay BiotechCo. Their base sequences are shown as follows:

ASO_1: 5′- *GGG GGG GGG GGGATT GTT AGC AGG ATT GCG GG*-3′

ASO_2: 5′- CCA ATG TGA TCT TTT GGT GTG GGG GGG GGG GG-3′

ASO_3: 5′- GGG GGG GGG GGG GGC CAA TGT TTG TAA TCA GT-3′

ASO_4: 5′- ATT TCC TTG GGT TTG TTC TGG GGG GGG GGG GG-3′

All oligonucleotide stock solutions were prepared with TE buffer and kept frozen until use.

2.2. Synthesis of (p)DNA-Templated AuNPs. A 20-base length antisense oligonucleotide strand was designed with extra 12 guanine to form AuNPs. A previous study[16] clearly demonstrated that polyguanine (G_{12}) tails had a reliable efficiency for the synthesis of polyvalent DNA@anisotropic AuNPs. Thus, based on this rapid method, 5 μL of $ASO_{1\ and\ 2\ \ and\ 3\ \ and\ 4}$ (100 μM) were added to 20 μL of HEPES buffer (5 mM), respectively, in four different reaction microtubes. Then 1 μL of $HAuCl_4$ (50 mM) was added to the mixtures. After a few seconds (about 10 s), the mixture color turned red.

2.3. SARS-CoV-2 Positive/Negative Sample Preparation. SARS-CoV-2 positive and negative throat swab samples were collected, and the total RNA was then extracted and purified in lysis buffer, in which the RNA extracted specimens were analyzed by RT-qPCR for N-gene (SARS-CoV-2 positive patients (n = 12) with Ct < 37 and SARS-CoV-2 negative samples (n = 9) with Ct > 37). However, the other collected throat samples were applied without any additional treatment and were heat-inactivated at 65 °C for 15 min, regardless of SARS-CoV-2 status (positive or negative). Then samples were used directly, without extraction and purification of RNA, to evaluate the performance of the proposed method. For this purpose, 10 μL of the clinical samples (as they are, without any prior processing) were added to 20 μL of a mixture containing 5 μL of synthesized ASO_1@AuNPs, ASO_2@AuNPs, ASO_3@AuNPs, and ASO_4@AuNPs, respectively. Then during the annealing process, the samples were incubated at room temperature for 5 min to form an ASOs-RNA heteroduplex.[17]

2.4. Preparation of the μPAD. The μPAD was easily fabricated by cutting the Whatman filter No.1. To prevent impurities, which could alter the results due to the interference effect, papers were immersed in deionized water for 1 day after being cut. To perform the sensing test, first, 5 μL of four ASO@AuNPs were immobilized on the detection zone by simple physical adsorption on paper, carried out by pouring a mixture (20 μL) of four ASO@AuNPs on the bare Whatman No.1 paper platform. Then, the coated paper was placed, in a solution containing the patient's throat swab sample, similar to a reported approach.[18]

https://doi.org/10.1021/acs.analchem.2c03544
Anal. Chem. 2022, 94, 13628−13634

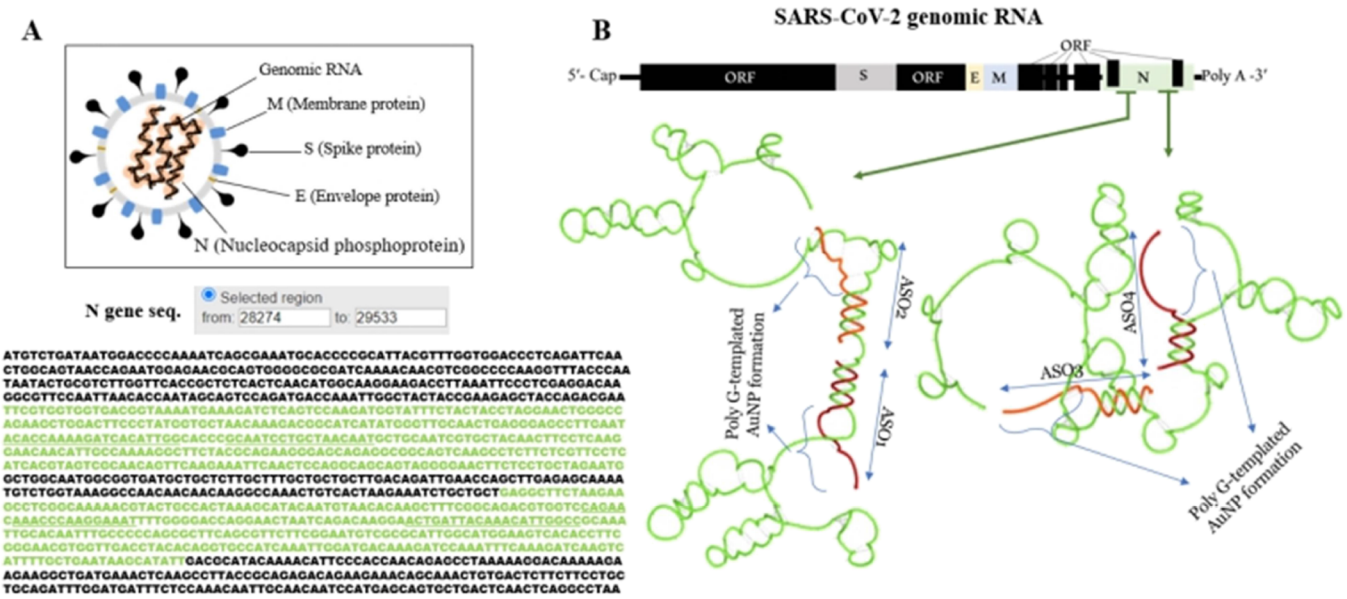

Figure 1. Schematic of the SARS-CoV-2 structure and the selected region of N-gene with its sequence are presented in (A). The proposed concept behind the aggregation of AuNPs, when capped with the ASOs, is schematically presented in (B); the assembly-guided structure simulated by NUPACK Analysis Algorithms. The most possible secondary structure with minimum free energy with ideal helical geometry for the complex of the selected region of N-gene (as linker) and four ASOs with extra strand poly G_{12} using the default algorithm parameters.

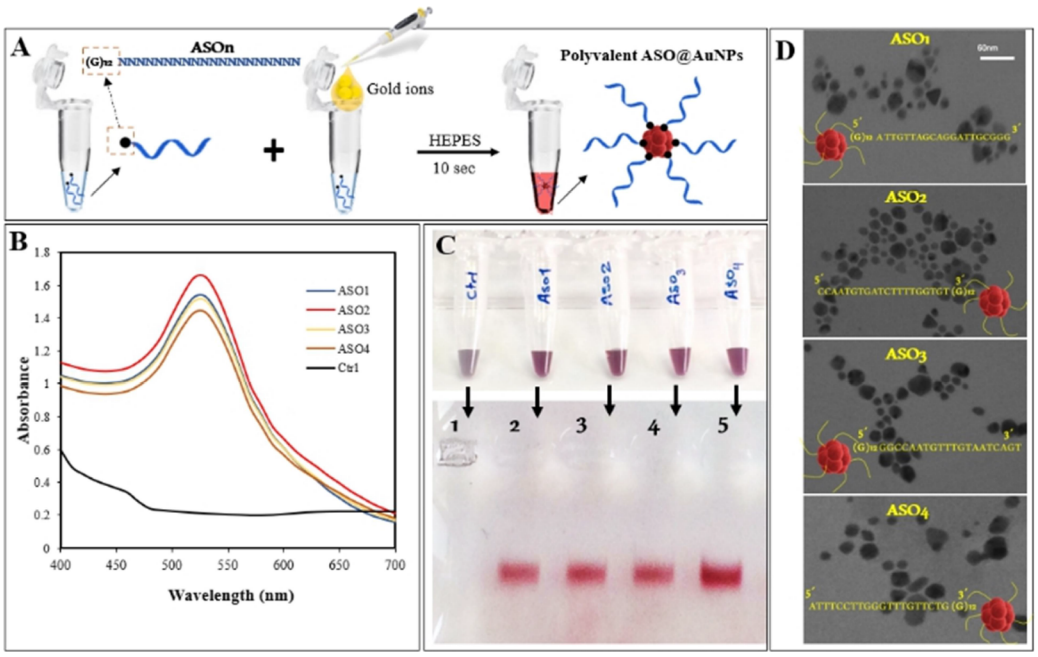

Figure 2. (A) Schematics of AuNP formation using extra strand poly G_{12} of ASOs as polyvalent. (B) Their absorption spectra. (C) Their photo under ambient light in the gel electrophoresis. (D) TEM images of the synthesized AuNPs using four ASOs.

3. RESULTS AND DISCUSSION

3.1. Design of the ASOs for Targeting SARS-CoV-2 Viral RNA. According to previous reports,[19] single-stranded RNA genome of SARS-CoV-2 comprises different open reading frames (ORFs) that encode several nonstructural proteins (Figure 1 (black boxes)) and four important structural proteins, including spike (S), envelope (E), membrane (M), and nucleocapsid (N) (as shown in Figure 1). Among the different regions of the genome, it is reported that some regions are more conserved such as the RNA-dependent RNA polymerase gene (RdRp) in the ORF1ab region and the E and N genes.[20] According to this, two regions of the N-gene (421−462 and 836−905) were selected as the target sequence for the selective detection of SARS-CoV-2, and four sets of ASOs were predicted as described in a previous report.[21]

In this design, optimal distances of ASOs from each other have been considered as this method is based on the proximity of plasmonic NPs and the subsequent changes in LSPR.[22] In addition, because of the aim of AuNP formation on the extra poly G strand, 12 guanine bases (G12) were added at the 5′ end of ASO_1 and ASO_3, whereas ASO_2 and ASO_4 had it at their 3′ ends (a detailed sequence has been provided in Section

https://doi.org/10.1021/acs.analchem.2c03544
Anal. Chem. 2022, 94, 13628−13634

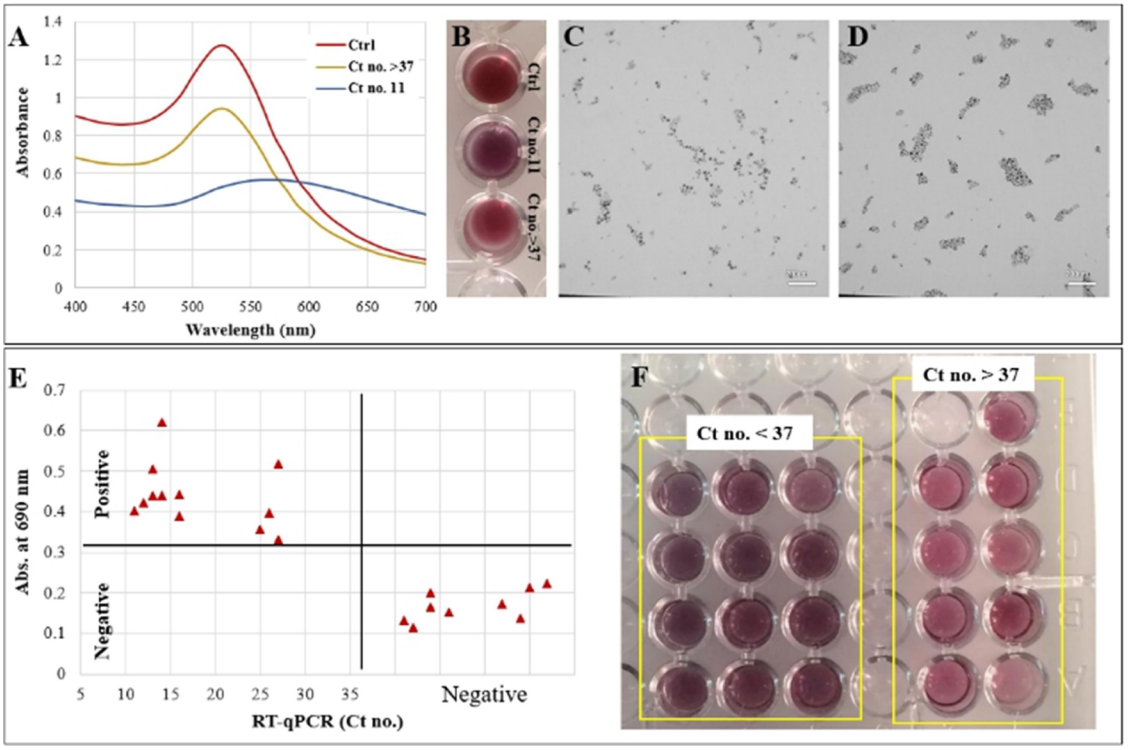

Figure 3. (A) UV−vis spectra of control (treated with buffer), positive (Ct no. 11), and negative (Ct no. > 37) extracted RNA throat swab samples in complex with ASO@AuNPs. (B) Photo showing them under visible light. TEM images of the reaction mixture with (C) negative and (D) positive samples. (E) Absorbance of the reaction mixture for 21 extracted RNA samples (12 positive and 9 negative) was recorded using a plate reader. The patient SARS-CoV-2 samples were initially tested using the FDA-approved RT-qPCR kit (LABGUN), and the results were plotted against our proposed signals. The horizontal threshold line indicates the minimum absorbance at 690 nm to indicate that the samples are viral positive by the proposed method. The vertical threshold line indicates that the maximum Ct number is about 37 to indicate that the sample is viral positive. (F) Inset photograph displaying them under visible light.

2.1). It was predicted that after in situ synthesis of four sets of ASO@AuNPs and in the presence of SARS-CoV-2 genome, the four sets of ASOs@AuNPs can form ASOs-RNA heteroduplex with the N-gene, which causes aggregation and color change of ASOs@AuNPs (Figure 1).

3.2. Characterization of Synthesized (p)ASOs@AuNPs. Four ASO strands with an extra poly G_{12} tail were investigated to find their ability to act as templates for the formation of AuNPs. In a simple method, they were mixed in $HAuCl_4$ and HEPES at five different reactions (one in the absence of any sequence, as control) (Figure 2A). After a few seconds, the samples turned red (except control sample), and they were imaged under ambient daylight as shown in Figure 2C. In addition, their optical behavior was characterized by studying their UV−vis absorption (400−700 nm). Their absorption spectra contained a prominent LSPR peak in the visible region around 530 nm, which is characteristic of the presence of AuNPs (Figure 2B).[10,11] Further evidence of AuNP formation was obtained by transmission electron microscopy (TEM) imaging. As revealed by the TEM analysis (Figure 2D), the anisotropic and spherical AuNP formation can be easily seen in four samples. It appears that the extra poly guanine (G12) tail at the end of each sequence can act as a template in the anisotropic and spherical AuNP formation.

Gel electrophoresis was also used to prove that the formed AuNPs are synthesized and attached to the ASO sequences. As shown in Figure 2C, four (p)ASO@AuNPS (lanes 2, 3, 4, and 5) moved in the gel, which could be attributed to conjugation of NPs with oligonucleotides, while the control sample (lane 1; in the absence of any sequence) remained in the well. Thus, these sequences were used for further investigation.

3.3. Analytical Performance. We tested four ASOs@AuNPs (ASO_1, ASO_2, ASO_3, and ASO_4) as colorimetric reporters, in the detection of RNA extracted from clinical oropharyngeal swab samples. As soon as addition of four ASOs@AuNPs to the RNA extracted mixture and without performing denaturing and annealing processes, the aggregation of AuNPs was visible, and after 15 min, this difference was more obvious. This causes a change in the LSPR peak such that the visible color of the solution changes from red to purple only in the presence of the extracted RNA sample from a positive (Ct no. < 37) patient (Figure 3A). As shown in Figure 3B, the visual results of the test can be monitored by the naked eye. TEM imaging was used to compare the aggregation intensity of in situ synthesized AuNPs with positive (Ct no. 11) and negative (Ct no. > 37) patient extracted RNA samples. The TEM images (Figure 3C,D) were also in close agreement with our previous readout and showed that anisotropic AuNPs had been aggregated by the positive sample (Figure 3D). The image in Figure 3C also showed that the AuNPs were dispersed in the negative patient sample.

Moreover, this sensing can be easily evaluated in a multiwell plate format, and the absorbance can be obtained using a conventional plate reader (Figure 3E). Figure 3F shows a clear color change that takes place in positive SARS-CoV-2 samples when extracted RNA samples are used.

3.4. Direct Quantification of Viral RNA in Patient Throat Samples. Lack of RNA extraction, amplification step,

https://doi.org/10.1021/acs.analchem.2c03544
Anal. Chem. 2022, 94, 13628−13634

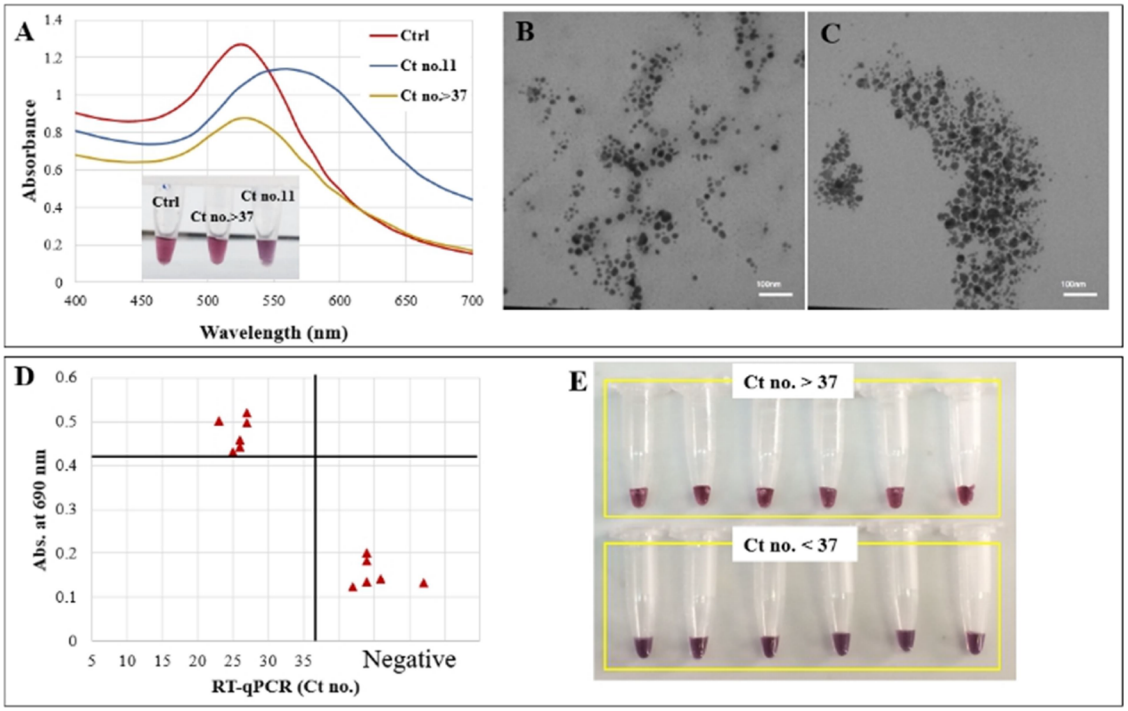

Figure 4. (A) UV−vis spectra of control (treated with buffer), positive (Ct no. 11), and negative (Ct no. > 37) throat swab samples without RNA extraction. Inset: photograph under visible light. TEM images of the reaction mixture with (B) negative and (C) positive samples. (D) Absorbance of the reaction mixture for 12 inactivated throat samples (6 positive and 6 negative) at 690 nm. The patient SARS-CoV-2 samples were initially tested using the RT-qPCR kit, and the results were plotted against our proposed signals. The horizontal threshold line indicates the minimum absorbance at 690 nm to indicate that the samples are viral positive by the proposed method. The vertical threshold line indicates that the maximum Ct number is about 37 to indicate that the sample is viral positive. (E) Inset photograph displaying them under visible light.

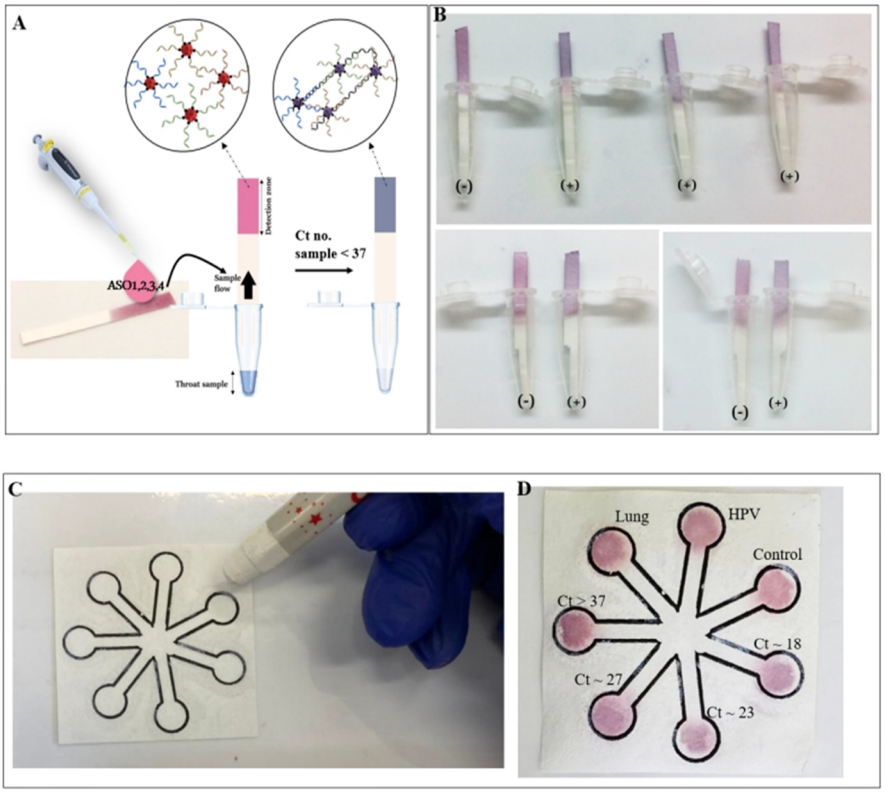

Figure 5. (A) Schematic illustration of μPAD fabrication using four ASO@AuNPs for colorimetric detection of viral RNA genome. (B) Color distribution and change on μPADs for SARS-CoV-2 detection in the presence of negative (−) and positive (+) samples. (C) Wax crayon-based μPAD and (D) their color change in the samples with Ct no. 18, 23, 27, HPV, and lung samples.

https://doi.org/10.1021/acs.analchem.2c03544
Anal. Chem. 2022, 94, 13628−13634

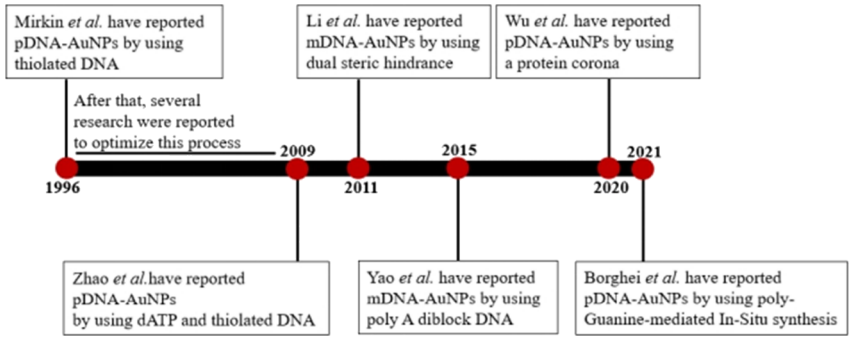

Figure 6. Timeline with some milestones of major development in DNA interaction with AuNPs.

Table 1. Recent Nanomaterial-Based Methods for Detection of SARS-CoV-2 Viral RNA Genome

detection method	labeled/ label-free	nanomaterial(s)	probe	sensing platform	ref.
electrochemical biosensor chip	labeled	graphene & gold nanoparticles	antisense oligonucleotide	using RNA extraction step/the digital electrochemical output	23
colorimetric test	label-free	reduced graphene oxide & carbon nanotube	DNA primers	nanocircuit integrated into an ingenious paper-based heater is (named HiPAD)/using LAMP step/visual detection	24
colorimetric/SERS/ fluorescence triple-mode sensor	labeled	gold nanoparticles	Cy3fluorophore-DNA probe	synthesized RNA target/the RNA target are spiked in TE buffer	20
colorimetric test	labeled	gold nanoparticles	CRISPR/Cas12a & DNA loop (hairpin)	using molecular transducer with isothermal amplification/ visual detection	25
colorimetric test	labeled	gold nanoparticles	thiolated-antisense oligonucleotide	using the RNA extraction step/using the signal amplification step/using RNase H enzyme/visual detection	21
colorimetric test	labeled	gold nanoparticles	thiolated-antisense oligonucleotide	RNA extraction-free/using isothermal nucleic acid amplification step/visual detection	26
colorimetric test	labeled	gold triangular nanoprisms	thiolated DNA probe	using the RNA extraction step/Au TNP-functionalized coverslip onto the glue area	27
colorimetric test	label-free	anisotropic gold nanoparticles	antisense oligonucleotide	RNA extraction-free/paper-based assay/direct-one-step naked-eye analysis	here

enzyme application, and lysis of samples in the current procedure are the main benefits, and this procedure does not require much time or special equipment and reagents. Thus, the performance of this method was evaluated directly on throat samples just after thermal inactivation. As shown in Figure 4A, the LSPR peak changes were measured in the presence of control (treat with buffer), positive (Ct no. < 37), and negative (Ct no. > 37) throat samples without RNA extraction. The characteristic LSPR peak of AuNPs at 530 nm shifts to longer wavelength at 575 nm in the presence of the positive sample, with a color change from red to purple.

In addition, the aggregation of AuNPs was determined through TEM images (Figure 4B,C), which show that the synthesized AuNPs are dispersed in the presence of the throat sample with Ct no. > 37, while in the presence of the patient sample with Ct no. < 37 they are strongly aggregated. As shown in Figure 4D, the SARS-CoV-2 samples were initially tested using RT-qPCR for N-gene, and the results were plotted against our LSPR signals at 690 nm. Color change is clearly seen in positive samples when thermally inactivated throat samples are used directly, without RNA extraction (Figure 4E).

These results show that four ASOs@AuNPs with high specificity and selectivity have been able to hybrid to their target, N-gene, in less than 5 min in such a complex solution.

3.5. Direct Detection with μPADs. The μPAD-based assays are good choices for detection, because they are fast, low-cost, easy-to-use and require low sample. Therefore, they are used for the detection of different targets in nonclinical environments such as airports, sports, and other centers. The μPAD-based assay used in this research and its corresponding color change are depicted in Figure 5A. It can be seen that in the presence of positive COVID19 samples, the color changes purple (Figure 5B). Hence, the developed method can be applied as a simple and rapid approach to build a point-of-care platform to diagnose different viral pathogens only by changing the ASO design.

To perform sensitivity and specificity studies, the wax crayon-based μPAD was used (Figure 5C). For this purpose, the circular zones were designed using Microsoft PowerPoint followed by ordinary ink printing. Then, outside of lines was drawn with a wax crayon to make a hydrophobic barrier to aqueous fluid. To perform the test, 5 μL of mixed probes (ASOs@AuNPs) were added in each circular zone, and after drying, 3 μL of samples containing SARS-CoV-2 virus with different Ct numbers and also samples containing HPV virus and RNA extracted from lungs were added to check the sensitivity and specificity, respectively. As shown in Figure 5D, the color change to purple in the samples with Ct no. 18, 23, and 27 is visible, and in the HPV and lung samples, there is no color change compared to the control which indicates the specificity of the method.

In comparison, the current method benefits from application of both nanotechnology approaches and use of a new method for the synthesis and conjugation of probes to NPs, which are compared in timeline in Figure 6 with more details. In addition, the current approach has several advantages compared to the alternative nanotechnology-based techniques, as detailed in Table 1.[20,21,23−28]

In summary, compared to previous reported methods in application of AuNPs for DNA/RNA detection as indicated in

https://doi.org/10.1021/acs.analchem.2c03544
Anal. Chem. 2022, 94, 13628−13634

a timeline (Figure 6), this method is cost-effective because it is label-free and the synthesis of gold is done in situ on the extra strand polyguanine oligonucleotide. On the other hand, it is fast because the synthesis is done in less than 10 s and does not need RNA extraction and amplification. It is user friendly because its use is limited to mixing the reaction components and the color changes are clear to the naked eye, while new systems such as CRISPR are based on PCR (RT-PCR) and fluorescent reporter or the smartphone-based electrochemical sensing systems need electrochemical detector and biosensor chip.[29−32] Simplicity of the new conjugation method with hybridization and annealing without amplification and denaturation steps enabled it to perform in the μPAD.

4. CONCLUSIONS

According to the results presented in this manuscript, four antisense oligonucleotides were designed with an additional G12 tail at the 5′ end of ASO_1 and ASO_3, and the 3′ end of ASO_2 and ASO_4, to act as a template for in situ formation of AuNPs. After formation of ASO@AuNPs, they were used for visible colorimetric sensing of the target N-gene due to the different LSPR peak without requirement of any complicated RNA extraction and amplification process. The applicability of this approach can be generalized to other viral RNAs by redesigning the antisense oligonucleotide probes against genome of the various pathogens.

AUTHOR INFORMATION

Corresponding Authors

Yasaman-Sadat Borghei − *Institute for Convergent Science and Technology, Sharif University of Technology, Tehran 11155-8639, Iran*; Email: yasamanborghei@ut.ac.ir

Saman Hosseinkhani − *Department of Biochemistry, Faculty of Biological Sciences, Tarbiat Modares University, Tehran 14115-154, Iran*; orcid.org/0000-0002-0345-7909; Phone: (98)-21-82884407; Email: saman_h@modares.ac.ir; Fax: (98)-21-82884484

Author

Hamid Reza Samadikhah − *Department of Biology, Faculty of Sciences, Central Tehran Branch, Islamic Azad University, Tehran 19585-466, Iran*

Complete contact information is available at: https://pubs.acs.org/10.1021/acs.analchem.2c03544

Notes

The authors declare no competing financial interest.

ACKNOWLEDGMENTS

Financial support of this work is provided by a grant (99007056) from Iran National Science Foundation (INSF).

REFERENCES

(1) Alvarez-Munoz, S.; Upegui-Porras, N.; Gomez, A. P.; Ramirez-Nieto, G. *Viruses* **2021**, *13*, 537.

(2) Carrasco-Hernandez, R.; Jácome, R.; López Vidal, Y.; Ponce de León, S. *ILAR J.* **2017**, *58*, 343−358.

(3) Woolhouse, M. E.; Brierley, L. *Sci. Data* **2018**, *5*, 80017.

(4) Ghaffari, M.; Mollazadeh-Bajestani, M.; Moztarzadeh, F.; Uludağ, H.; Hardy, J. G.; Mozafari, M. *Emergent Mater.* **2021**, *4*, 19−34.

(5) Kriegova, E.; Fillerova, R.; Kvapil, P. *Diagnostics* **2020**, *10*, 605.

(6) Ventura, B. D.; Cennamo, M.; Minopoli, A.; Campanile, R.; Censi, S. B.; Terracciano, D.; Portella, G.; Velotta, R. *ACS Sens.* **2020**, *5*, 3043−3048.

(7) Rabe, B. A.; Cepko, C. *Proc. Natl. Acad. Sci. U. S. A.* **2020**, *117*, 24450−24458.

(8) Gupta, R.; Sagar, P.; Priyadarshi, N.; Kaul, S.; Sandhir, R.; Rishi, V.; Singhal, N. K. *Front. Nanotechnol.* **2020**, *2*, 6.

(9) Iravani, S. *Mater. Adv.* **2020**, *1*, 3092−3103.

(10) Borghei, Y. S.; Hosseini, M.; Dadmehr, M.; Hosseinkhani, S.; Ganjali, M. R.; Sheikhnejad, R. *Anal. Chim. Acta* **2016**, *904*, 92−97.

(11) Borghei, Y. S.; Hosseini, M.; Ganjali, M. R.; Ju, H. *Microchim. Acta* **2018**, *185*, 286.

(12) Mirkin, C. A.; Letsinger, R. L.; Mucic, R. C.; Storhoff, J. J. *Nature* **1996**, *382*, 607−609.

(13) Zhao, W.; Lin, L.; Hsing, I. M. *Bioconjugate Chem.* **2009**, *20*, 1218−1222.

(14) Yao, G.; Pei, H.; Li, J.; Zhao, Y.; Zhu, D.; Zhang, Y.; Lin, Y.; Huang, Q.; Fan, C. *NPG Asia Mater.* **2015**, *7*, No. e159.

(15) Wu, R.; Peng, H.; Zhu, J. J.; Jiang, L. P.; Liu, J. *Front. Chem.* **2020**, *8*, 121.

(16) Borghei, Y. S.; Hosseinkhani, S. *Photochem. Photobiol.* **2022**, DOI: 10.1111/php.13586.

(17) Borghei, Y. S.; Hosseini, M.; Ganjali, M. R. *Sens. Actuators, B* **2018**, *273*, 1618−1626.

(18) Borghei, Y. S.; Hosseini, M. *RSC Adv.* **2018**, *8*, 30148−30154.

(19) Nguyen, T. T.; Pathirana, P. N.; Nguyen, T.; Nguyen, Q. V. H.; Bhatti, A.; Nguyen, D. C.; Nguyen, D. T.; Nguyen, N. D.; Creighton, D.; Abdelrazek, M. *Sci. Rep.* **2021**, *11*, 3487.

(20) Gao, Y.; Han, Y.; Wang, C.; Qiang, L.; Gao, J.; Wang, Y.; Liu, H.; Han, L.; Zhang, Y. *Anal. Chim. Acta* **2021**, *1154*, No. 338330.

(21) Moitra, P.; Alafeef, M.; Dighe, K.; Frieman, M. B.; Pan, D. *ACS Nano* **2020**, *14*, 7617−7627.

(22) Borghei, Y. S.; Hosseini, M. *Sci. Rep.* **2019**, *9*, 5453.

(23) Alafeef, M.; Dighe, K.; Moitra, P.; Pan, D. *ACS Nano* **2020**, *14*, 17028−17045.

(24) Li, S.; Huang, S.; Ke, Y.; Chen, H.; Dang, J.; Huang, C.; Liu, W.; Cui, D.; Wang, J.; Zhi, X.; Ding, X. *Adv. Funct. Mater.* **2021**, *31*, No. 2100801.

(25) Chrisá Le, X. Y. *Chem. Commun.* **2021**, *57*, 6871−6874.

(26) Alafeef, M.; Moitra, P.; Dighe, K.; Pan, D. *Nat. Protoc.* **2021**, *16*, 3141−3162.

(27) Masterson, A. N.; Muhoberac, B. B.; Gopinadhan, A.; Wilde, D. J.; Deiss, F. T.; John, C. C.; Sardar, R. *Anal. Chem.* **2021**, *93*, 8754−8763.

(28) Yan, S.; Ahmad, K. Z.; Warden, A. R.; Ke, Y.; Maboyi, N.; Zhi, X.; Ding, X. *Biosens. Bioelectron.* **2021**, *193*, No. 113535.

(29) Liang, Y.; Lin, H.; Zou, L.; Deng, X.; Tang, S. *Biosens. Bioelectron.* **2022**, *205*, No. 114098.

(30) Fozouni, P.; Son, S.; de León Derby, M. D.; Knott, G. J.; Gray, C. N.; D'Ambrosio, M. V.; Zhao, C.; Switz, N. A.; Kumar, G. R.; Stephens, S. I.; Boehm, D. *Cell* **2021**, *184*, 323−333.e9.

(31) Dou, Y.; Su, J.; Chen, S.; Li, T.; Wang, L.; Ding, X.; Song, S.; Fan, C. *Chem. Commun.* **2022**, *58*, 6108−6111.

(32) Yang, L. F.; Kacherovsky, N.; Panpradist, N.; Wan, R.; Liang, J.; Zhang, B.; Salipante, S. J.; Lutz, B. R.; Pun, S. H. *Anal. Chem.* **2022**, *94*, 7278.